Field-Effect Transistors

DOI: 10.1002/ange.201001683

High-Performance Langmuir–Blodgett Monolayer Transistors with High Responsivity**

Yang Cao, Zhongming Wei, Song Liu, Lin Gan, Xuefeng Guo, Wei Xu, Michael L. Steigerwald, Zhongfan Liu,* and Daoben Zhu**

Shrinking the dimensions of organic field-effect transistors (OFETs) down to the nanometer scale offers new, defect-free charge transport regimes. This may lead to the improvement of the device performance, such as larger carrier mobilities, increased device speed, lower power dissipation, and enhanced on/off ratios. Therefore, much effort has recently been made to scale down both the thickness of the OFET devices (the semiconductor and/or insulator layers)[1] and their lateral dimension (source–drain distance).[2] With size reduction, however, the device performance is mainly hampered by the parasitic contact resistances with a high injection barriers and the poor long-range order of organic semiconductors. Most commonly, gold source–drain (S/D) electrodes are used as the charge-injecting metal in organic electronic devices. Gold is used because of its chemical stability and its work function that matches the energy level of organic semiconductors in most cases, thus lowering the Schottky barriers. To reduce the contact resistance, several alternative materials, including carbon nanotubes (CNTs),[3] carbon nanotube/polymer nanocomposites,[4] graphene multilayers,[5] and conductive polymers,[6] have been utilized as potential substitutes for the expensive gold S/D electrodes. On the other hand, molecular organization can be improved by forming dense and well-ordered self-assembled monolayers through bottom-up approaches,[7] as illustrated by the work of Smits et al.[7d] To optimize the performance of OFETs, device fabrication should be considered as a holistic process. The electrode materials, the contact surface, and device fabrication are so closely interrelated that they cannot be optimized independently. To date, only few examples of OFETs have been demonstrated to achieve high-performance by holistic consideration of all these parameters.[8]

With this in mind, herein we present a new class of high-performance photoresponsive molecular field-effect transistors formed from Langmuir–Blodgett (LB) monolayers of copper phthalocyanine (CuPc), using two-dimensional (2D) ballistically-conductive single-layer graphene as planar contacts. The unique feature detailed herein is the integration of LB techniques with the fabrication of nanogap electrodes to build functional molecular electronic devices. LB techniques offer a promising and reliable method to prepare large-area ordered ultrathin films with well-defined architectures. In previous work, we and others[9] have demonstrated the successful applications of the LB technique to CuPc and conjugated polymers in producing ultrathin film OFETs. However, the charge carrier mobilities μ in these devices were low, namely about 10^{-7}–10^{-3} $cm^2 V^{-1} s^{-1}$. This might be mainly ascribed to the high contact resistance when gold was used for S/D electrodes and to the defects in the micrometer-long channels. For this study, we employed single-layer graphene as S/D nanoelectrodes to overcome these difficulties. This choice is because graphene, a new class of 2D carbon nanostructure, holds a set of remarkable electronic and physical properties,[10] such as ballistic transport with low resistivity, high chemical stability, and high mechanical strength. Recently, we developed a reliable method of oxidatively cutting single-layer graphene as ideal 2D contacts for producing nanoscale organic transistors.[11] Due to the reduced hole-injection barrier and the large contact area, these devices showed bulk-like FET properties ($\mu \approx 10^{-3}$ $cm^2 V^{-1} s^{-1}$). In the current work, we present a combined method based on the holistic consideration mentioned above. The significant improvement is that this method gives almost 100 percent yields of working monolayer transistors with higher carrier mobility, higher on/off ratio, and reliable reproducibility. We also present the details of their very sensitive photoresponsive behavior, which has never been reported before in monolayer transistors.

The structure of CuPc monolayer transistors is illustrated in Figure 1. The fabrication of cut 2D graphene nanogap electrodes was detailed in our previous work.[11] In brief, three-terminal graphene-based transistors were first made by the combination of a peeling-off technique and electron beam

[*] Y. Cao, S. Liu, L. Gan, Prof. X. Guo, Prof. Z. Liu
Beijing National Laboratory for Molecular Sciences
State Key Laboratory for Structural Chemistry of Unstable and Stable Species
College of Chemistry and Molecular Engineering, Peking University
Beijing 100871 (P. R. China)
Fax: (+86) 10-6275-7789
E-mail: guoxf@pku.edu.cn
zfliu@pku.edu.cn

Z. Wei, Prof. W. Xu, Prof. D. Zhu
Beijing National Laboratory for Molecular Sciences
Institute of Chemistry, Chinese Academy of Sciences
00190 Beijing (P. R. China)
E-mail: zhudb@iccas.ac.cn

M. L. Steigerwald
Department of Chemistry and
The Columbia University Energy Frontiers Research Center
Columbia University, New York, NY 10027 (USA)

[**] We are grateful to C. Nuckolls from Columbia University for his help and enlightening discussions. We acknowledge primary financial support from FANEDD (No. 2007B21), MOST (2009CB623703 and 2008AA062503) and NSFC (Grant No. 50873004, 50821061, and 20833001).

Supporting information for this article is available on the WWW under http://dx.doi.org/10.1002/anie.201001683.

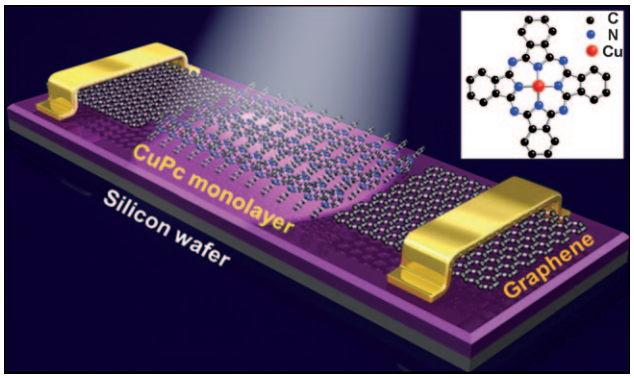

Figure 1. The structure of the CuPc monolayer transistor device with metal electrodes protected by a 50 nm layer of silicon dioxide. Inset: the molecular structure of copper phthalocyanine (CuPc).

(e-beam) lithography on a heavily doped silicon wafer substrate with a 300 nm layer of thermally grown oxide. In Figure 2a, we show optical micrographs of a representative integrated circuit along with the atomic force microscopy (AFM) image of the graphene sheets, with a gap size of about 50 nm in the circuit. Typically, the average thickness of graphene used in this study is 0.5–0.9 nm, which corresponds to a single layer graphene. To rule out the possibility of charge transfer through metal electrodes, we protected Au/Cr metal electrodes (40 nm/3 nm, patterned by e-beam lithography) by a 50 nm layer of silicon dioxide deposited by e-beam thermal evaporation before photoresist liftoff. After the electrical characterization of these transistors (Figure 2b, black), we

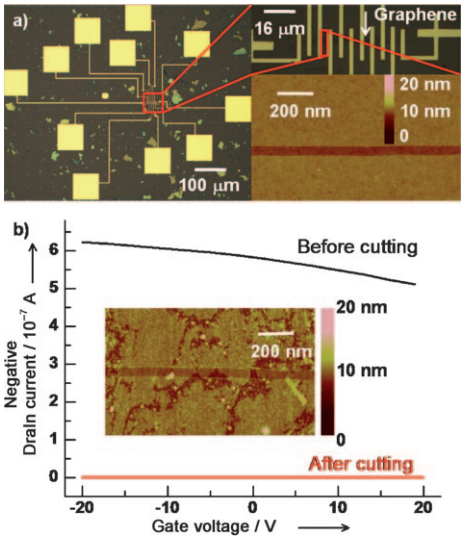

Figure 2. Graphene sheets functioning as planar contacts. a) Optical micrographs and an AFM image of a representative device before monolayer deposition. The gap size is about 50 nm. The thickness of graphene is about 0.7 nm, which corresponds to a single layer. Inset: height profile. b) Electrical characteristics of the same graphene sheet (drain current I_D vs. gate bais voltage V_G at $V_D = -500$ μV) used for testing before and after oxidative cutting. Inset: AFM image of the same graphene sheet after monolayer deposition (monolayer height: ca. 1.3 nm). (see Supporting Information for more details of the images).

then oxidatively cut individual graphene sheets using another ultrafine lithographic process and precise oxygen plasma etching. This step produces nanogaps between the graphene half-sheets. Owing to the nanogaps, the devices showed no conductance down to the noise limit of the measurement (ca. 100 fA) (Figure 2b, red). We controlled the fabrication process to give a gap size in the range of 20–100 nm. Each pair of graphene half-sheets serves as a set of S/D nanoelectrodes. Finally, CuPc monolayers were vertically transferred onto the substrate surface through the conventional LB technique (see the Supporting Information).[9b,c] We found that homogenous high-coverage LB monolayers (height ca. 1.3 nm) were easily formed in a face-to-face closely stacking fashion with a tilted angle of 60.4° (Figure 2b, inset).[9c] By applying gate bias voltages (V_G) from the global back-gate (the doped silicon wafer), we were able to fine-tune the carrier density in the devices.

Once CuPc LB monolayers were deposited to contact graphene electrodes with nanogaps, all of the resultant nanodevices behave as p-type, hole-transporting semiconductors. A set of typical transistor characteristics for the same device in Figure 2 are shown in Figure 3. As Au/Cr metal

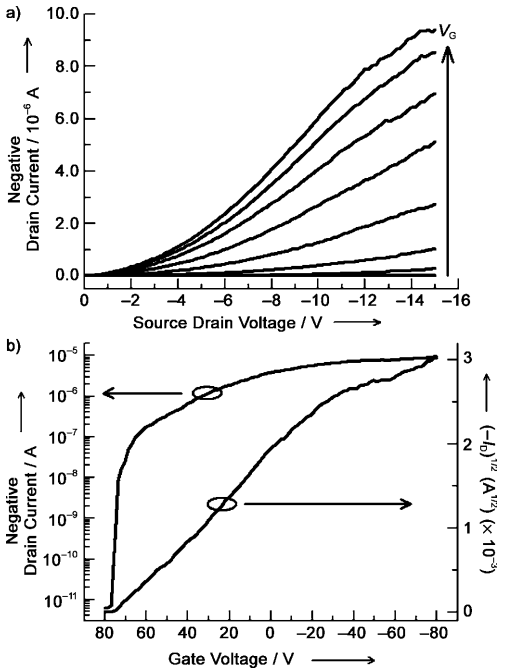

Figure 3. Characteristics of a representative device shown in Figure 2: a) Output characteristics ($V_G = 80 \rightarrow -88$ V in -24 V steps) and b) transfer characteristics (drain voltage $V_D = -15$ V; channel length (L) = 50 nm; channel width (W) = 2 μm.

electrodes have been protected by silicon dioxide, it is clear that the only pathway for charge transport is through graphene electrodes bridged by CuPc LB monolayers.[8,11] Figure 3a shows output characteristics of the device as a function of gate bias. At the high negative gate voltage bias, we observed the superlinear increase in the drain current I_D with S/D voltages V_D at low values; when V_D reaches -15 V, the current almost reaches saturation. Considering these

observations, we extracted the carrier mobilities in both unsaturation and saturation modes from the drop of transfer characteristics of the device in Figure 3b (see the Supporting Information).[12] The calculated unsaturation and saturation mobilities are about $0.04\,cm^2V^{-1}s^{-1}$ and about $0.01\,cm^2V^{-1}s^{-1}$, respectively. Further work demonstrated that the unsaturation mobilities remain constant at the different S/D voltage biases (−5, −8, −10, and −15 V). These values are ranked the highest among those obtained from organic ultrathin-film transistors,[7a,d,9] and are much higher than those obtained from bulk-like OFETs fabricated with conventional methods at room temperature (10^{-5}–$10^{-3}\,cm^2V^{-1}s^{-1}$).[13] Although comparable mobilities could be achieved, the fabrication processes required the high substrate temperature ($\geq 125\,^{\circ}C$) through complex vacuum evaporation,[13,14] rather than simple solution processing. This is significant, considering that the charge-transfer transport in our monolayer transistors occurs from a single 1.3 nm-thick layer. Another special feature of CuPc LB monolayer transistors is that the transfer curve in Figure 3b shows a current modulation of over six orders of magnitude. This value is more than three orders of magnitude higher than those of monolayer transistors of CuPc LB films based on metal electrodes.[9b] This explains how device characteristics of these nanodevices can be efficiently controlled by the gate voltage bias, even with a thick gate dielectric (300 nm in our case). Both the mobility and on/off ratio are the critical parameters in evaluating the quality of OFETs, and it has proved difficult to achieve such high values of these parameters in nanoscale devices made with metal electrodes.[2,12] However, at positive gate voltage biases, we only observed the superlinear current increase with S/D voltages (Figure 3a), which implies that our devices are still influenced to some extent by short channel effects that result from insufficient gate coupling in devices having a 300 nm thick gate dielectric.[1,2] This deficiency leaves room for future improvement of the device performance by scaling down OFETs for both the dielectric thickness and the channel length.

Along with the high carrier mobility and the high on/off ratio described above, the yield of working devices is quite high (almost 50 out of around 50 devices), making these results extremely reproducible. In general, because of the limited bottom-up self-assembly approaches and the difficulty of the formation of densely-stacked large-area monolayers, the device performance and the yield are largely restricted.[7a,b,d,8b] We suggest that LB technology, in combination with the 2D graphene contacts, yields the observed high-performance FET behaviors of devices with high reproducibility. The LB technique is an efficient bottom-up approach by which to fabricate large-area well-organized monolayers at the molecular level. In particular, in the current case, CuPc is chosen to form uniform monolayers with the face-to-face π–π stacking conformation,[9a–c] which is favorable for charge transport. On the other hand, we use single-layer graphene, which have the similar molecular structure with molecules, as 2D ballistic planar contacts in these devices. In such devices, aromatic compounds are able to form the strong interactions with graphene in a two-dimensional direction, which in turn helps molecules orient themselves along the nanogaps. Due to the low work function of graphene (4.7–4.9 eV),[5,11] graphene sheets are ideal electrodes with excellent interface contact with molecules and reduced injection barriers. CuPc–graphene nanotransistors displayed output currents (Supporting Information, Figure S2) that are about three orders of magnitude greater than that for similar gold-contacted devices, thus proving that OFETs based on graphene electrodes exhibited reduced injection barriers and overall better effective mobilities. Consequently, we infer that the synergistic combination of CuPc monolayer molecular conformation and the 2D planar structural nature of graphene electrodes makes a major contribution to the better performance of these devices. The threshold voltage V_T in these devices is large (ca. +75 V), which is probably due to the shortened channel length and/or the high density of carrier traps at the interface between bare SiO_2 and CuPc. The calculated subthreshold swing S from the device is about 500 mV per decade (Figure 3), which is similar to the values obtained from those using carbon nanotube point contacts.[3b,8] Interestingly, although the length of nanogaps (effective channel length) varied considerably from device to device (from 20 to 100 nm), no obvious relation was found between the length and the transistor characteristics of the devices. Due to the inevitable variables in devices, such as the geometry of graphene and the quality of CuPc LB monolayers, the carrier mobility varied from 0.01 to $0.04\,cm^2V^{-1}s^{-1}$ and the on/off ratio from 10^5 to 10^6.

Because the active channel of the transistors consists of photoactive CuPc monolayers that are exposed to the environment, they are sensitive to external stimuli, such as light.[15] We were able to measure their DC photoconductivity at room temperature in ambient atmosphere under light illumination, which is surprising, because the photocurrent in the devices occurs within a single 1.3 nm-thick layer. In general, it is difficult to detect the photoresponsive properties of monolayer transistors because of instantaneous detrimental charge recombination under light irradiation and the quenching of the photoexcited states of monolayer molecules exposed to the environments.[7,8b] As discussed above, graphene sheets can form the excellent interface contact with molecules and exhibit barrier-free-like injection. Therefore, the application of relatively small voltages yields efficient charge injection in the gap area in the current case. This could significantly avoid detrimental charge recombination under light irradiation and the quenching effect by the environments, thus affording efficient charge transport through graphene contacts at low voltages. The reversible photocurrent of the same device shown in Figure 2 under irradiation of visible light (150 W halogen lamp) was stable without obvious degradations over many measurement cycles, even in the presence of oxygen and moisture in the air (Supporting Information, Figure S3). However, the response time is low (about 40 seconds), which is probably due to the diffusion processes and/or large capacitive components. The power dependence of the photocurrent of the same device is shown in Figure 4a. With the increase of light power, the drain current I_D of the device gradually saturates, indicating that the photoinduced carrier density reaches its maximum.

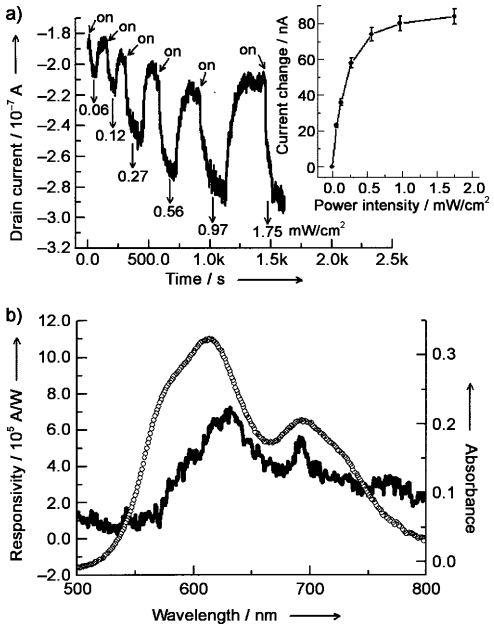

Figure 4. Photoresponsive behavior of the same device as in Figure 2. a) The time dependence of the drain current I_D as lights of different power are switched on and off. Inset: power dependence of the changes in I_D. $V_G = 0$ V and $V_D = -8$ V. b) Comparison of the wavelength-dependent spectrum (——) with the UV/Vis absorption spectrum (○) of CuPc thin films. Light was scanned from 500 to 800 nm in 5 nm steps with each wavelength left on for 5 seconds. All wavelengths used were adjusted to be constant (Ilight = 30 μW cm^{-2}). $V_G = 0$ V and $V_D = -6$ V; $W = 2$ μm, $L = 50$ nm.

To ensure that the path of photocurrent is through the nanojunctions between graphene electrodes and CuPc monolayers, we tested a number of devices that have been fully cut but lack CuPc monolayers. All of these devices behave as open circuits with no field effect induced by the gate electrode. To further understand the important role of CuPc monolayers in device photoconductivity, we carried out wavelength-dependent measurements. Based on the device photocurrent, we calculated the responsivities to indicate the intrinsic photosensitivity of the devices (see the Supporting Information). The calculated responsivities as a function of light wavelength of the same device have been shown in Figure 4b while the device was held at $V_G = 0$ V and $V_D = -6$ V (light intensity $I_{Light} \approx 30$ μW/cm^2, $W = 2$ μm and $L = 50$ nm). The peak in the responsivity spectrum for the device at about 625 nm matches that of the UV/Vis absorption spectrum in the Q-band region of 50 nm thick CuPc films deposited by thermal evaporation. This is attributed to the π–π* transition of CuPc aggregated species formed by face-to-face stacking.[9a] The weak shoulder at about 690 nm observed at the lower-energy side of the responsivity spectrum is ascribed to the π–π* transition of CuPc monomers. Control experiments using either uncut bare graphene transistors or uncut graphene transistors covered with a CuPc LB monolayer demonstrated that the devices showed no effect when irradiated with any light (visible light from the halogen lamp, light with different power, or light with different wavelengths; see the Supporting Information). These results without doubt show that CuPc LB monolayers in the nanogaps play the key role in device characteristics. The best responsivity of the device is superhigh, at about 7.10×10^5 A W^{-1}. This strong photoresponse might be due to an integrated mechanism, for example, owing to build-up of electron-trapped charges at the semiconductor/dielectric interface during illumination over tens of seconds. However, these values are only for comparison with conventional photodetectors (typically < 10 A W^{-1}), because we use the same conventional model for the calculation,[16] which might be not accurate in the present case.

In summary, we have demonstrated a universal approach of holistic device fabrication. The integration of LB techniques with sophisticated micro/nanofabrication affords efficacious molecular field-effect transistors with bulk-like carrier mobility (as high as 0.04 cm^2 V^{-1} s^{-1}), high on/off current ratios (over 10^6), high yields (almost 100%), and high reproducibility. These transistors are formed from self-assembled uniform monolayers of p-type CuPc semiconductors using single-layer graphene as planar contacts. Another important result is that these transistors are ultrasensitive to light, although their active channel consists of only a single 1.3 nm-thick layer, forming the basis for new types of environmental sensors and tunable photodetectors. This method of incorporating molecular functionalities into molecular electronic devices by combining bottom-up self-assembly and top-down device fabrication should speed the development of nanometer/molecular electronics in the future.

Received: March 21, 2010
Revised: May 16, 2010
Published online: July 14, 2010

Keywords: field-effect transistors · graphene · molecular devices · monolayers · photoresponsivity

[1] a) S. A. DiBenedetto, A. Facchetti, M. A. Ratner, T. J. Marks, *Adv. Mater.* **2009**, *21*, 1407–1433; b) A. L. Briseno, S. C. B. Mannsfeld, S. A. Jenekhe, Z. Bao, Y. Xia, *Mater. Today* **2008**, *11*, 38–47; c) Q. Tang, L. Jiang, Y. Tong, H. Li, Y. Liu, Z. Wang, W. Hu, Y. Liu, D. Zhu, *Adv. Mater.* **2008**, *20*, 2947–2951; d) A. Facchetti, M.-H. Yoon, T. J. Marks, *Adv. Mater.* **2005**, *17*, 1705–1725.

[2] Y. Cao, M. L. Steigerwald, C. Nuckolls, X. Guo, *Adv. Mater.* **2010**, *22*, 20–32.

[3] a) K. Tsukagoshi, I. Yagi, Y. Aoyagi, *Appl. Phys. Lett.* **2004**, *85*, 1021–1023; b) P. Qi, Javey, Rolandi, Q. Wang, E. Yenilmez, H. Dai, *J. Am. Chem. Soc.* **2004**, *126*, 11774–11775; c) C. M. Aguirre, C. Ternon, M. Paillet, P. Desjardins, R. Martel, *Nano Lett.* **2009**, *9*, 1457–1461; d) Y. Y. Zhang, Y. Shi, F. Chen, S. G. Mhaisalkar, L.-J. Li, B. S. Ong, Y. Wu, *Appl. Phys. Lett.* **2007**, *91*, 223511; e) Q. Cao, S.-H. Hur, Z.-T. Zhu, Y. Sun, C. Wang, M. A. Meitl, M. Shim, J. A. Rogers, *Adv. Mater.* **2006**, *18*, 304–309.

[4] a) M. Lefenfeld, G. Blanchet, J. A. Rogers, *Adv. Mater.* **2003**, *15*, 1188–1191; b) J. Sung, P. S. Jo, H. Shin, J. Huh, B. G. Min, D. H. Kim, C. Park, *Adv. Mater.* **2008**, *20*, 1505–1510.

[5] a) C.-A. Di, D. Wei, G. Yu, Y. Liu, Y. Guo, D. Zhu, *Adv. Mater.* **2008**, *20*, 3289–3293; b) S. Pang, H. N. Tsao, X. Feng, K. Müllen, *Adv. Mater.* **2009**, *21*, 3488–3491.

[6] a) X. H. Zhang, S. M. Lee, B. Domercq, B. Kippelen, *Appl. Phys. Lett.* **2008**, *92*, 243301; b) F. Xue, Y. Su, K. Varahramyan, *IEEE Trans. Electron Devices* **2005**, *52*, 1982 – 1987.

[7] a) M. Mottaghi, P. Lang, F. Rodriguez, A. Rumyantseva, A. Yassar, G. Horowitz, S. Lenfant, D. Tondelier, D. Vuillaume, *Adv. Funct. Mater.* **2007**, *17*, 597 – 604; b) G. S. Tulevski, Q. Miao, Fukuto, R. Abram, B. Ocko, R. Pindak, M. L. Steigerwald, C. R. Kagan, C. Nuckolls, *J. Am. Chem. Soc.* **2004**, *126*, 15048 – 15050; c) C. R. Kagan, Afzali, R. Martel, Gignac, P. M. Solomon, Schrott, B. Ek, *Nano Lett.* **2003**, *3*, 119 – 124; d) C. P. E. Smits, S. G. Mathijssen, P. A. van Hal, S. Setayesh, T. T. C. Geuns, K. A. H. . Mutsaers, E. Cantatore, H. J. Wondergem, O. Werzer, R. Resel, Kemerink, S. Kirchmeyer, A. M. Muzafarov, S. A. Ponomarenko, B. de Boer, P. W. M. Blom, D. M. de Leeuw, *Nature* **2008**, *455*, 956 – 959.

[8] a) X. Guo, S. Xiao, M. Myers, Q. Miao, M. L. Steigerwald, C. Nuckolls, *Proc. Natl. Acad. Sci. USA* **2009**, *106*, 691 – 696; b) X. Guo, M. Myers, S. Xiao, M. Lefenfeld, R. Steiner, G. S. Tulevski, J. Tang, B J. aumert, F. Leibfarth, J. T. Yardley, M. L. Steigerwald, P. Kim, C. Nuckolls, *Proc. Natl. Acad. Sci. USA* **2006**, *103*, 11452 – 11456.

[9] a) K. Xiao, Y. Liu, X. Huang, Y. Xu, G. Yu, D. Zhu, *J. Phys. Chem. B* **2003**, *107*, 9226 – 9230; b) Z. Wei, Y. Cao, W. Ma, C. Wang, W. Xu, X. Guo, W. Hu, D. Zhu, *Appl. Phys. Lett.* **2009**, *95*, 033301; c) Z. Wei, W. Xu, W. Hu, D. Zhu, *Langmuir* **2009**, *25*, 3349 – 3351; d) G. Xu, Z. Bao, J. T. Groves, *Langmuir* **2000**, *16*, 1834 – 1841; e) J. Paloheimo, P. Kuivalainen, H. Stubb, E. Vuorimaa, P. Yli-Lahti, *Appl. Phys. Lett.* **1990**, *56*, 1157 – 1159; f) L. Aguilhon, J. P. Bourgoin, A. Barraud, P. Hesto, *Synth. Met.* **1995**, *71*, 1971 – 1974.

[10] a) A. K. Geim, K. S. Novoselov, *Nat. Mater.* **2007**, *6*, 183 – 191; b) C. Lee, X. Wei, J. W. Kysar, J. Hone, *Science* **2008**, *321*, 385 – 388; c) M. Y. Han, B. Oezyilmaz, Y. Zhang, P. Kim, *Phys. Rev. Lett.* **2007**, *98*, 206801.

[11] Y. Cao, S. Liu, Q. Shen, K. Yan, P. Li, J. Xu, D. Yu, M. L. Steiger wald, C. Nuckolls, Z. Liu, X. Guo, *Adv. Funct. Mater.* **2009**, *19*, 2743 – 2748.

[12] C. D. Dimitrakopoulos, P. R. L. Malenfant, *Adv. Mater.* **2002**, *14*, 99 – 117.

[13] Z. Bao, A. J. Lovinger, A. Dodabalapur, *Appl. Phys. Lett.* **1996**, *69*, 3066 – 3068.

[14] a) J. Zhang, J. Wang, H. Wang, D. Yan, *Appl. Phys. Lett.* **2004**, *84*, 142 – 144; b) J. Yuan, J. Zhang, J. Wang, X. Yan, D. Yan, W. Xu, *Appl. Phys. Lett.* **2003**, *82*, 3967 – 3969; c) M. Ofuji, K. Ishikawa, H. Takezoe, K. Inaba, K. Omote, *Appl. Phys. Lett.* **2005**, *86*, 062114.

[15] a) N. Minami, *J. Chem. Soc. Faraday Trans. 2* **1982**, *78*, 1871 – 1880; b) T. Tanaka, M. Matazuma, R. Hirohashi, *Thin Solid Films* **1998**, *322*, 290 – 297.

[16] M. C. Hamilton, S. Martin, J. Kanicki, *IEEE Trans. Electron Devices* **2004**, *51*, 877 – 885.

